AIAA JOURNAL
Vol. 42, No. 1, January 2004

Alleviation of Airfoil Dynamic Stall Moments via Trailing-Edge-Flap Flow Control

Daniel Feszty,* Eric A. Gillies,† and Marco Vezza‡
University of Glasgow, Glasgow, Scotland G12 8QQ, United Kingdom

Trailing-edge-flap flow control for the mitigation of large negative pitching moments and negative aerodynamic damping caused by helicopter rotor blade dynamic stall was studied by means of computational fluid dynamics. A discrete vortex method was used for the simulations. The model geometry was a NACA 0012 airfoil oscillating in an $\alpha(t) = 15$ deg + 10 deg sin(ωt) motion at the reduced frequency of $k = 0.173$. The freestream flow conditions were of $M = 0.117$ and $Re = 1.463296 \times 10^6$. The flap actuation was a brief pulse signal of a sinusoidal shape, and it was shown that for optimum results upward flap deflections of the duration of about the $\frac{1}{3}$ of the airfoil motion time period and start time in the third quarter of the azimuth should be applied. Detailed analysis of the flowfield showed that the trailing-edge vortex (TEV), induced by the downstream convecting dynamic stall vortex was in fact responsible for the large negative pitching moments and associated negative damping. The suggested flow control technique displaced the TEV to a higher location, from where its wash down could take place more rapidly. The general applicability of the method was demonstrated on a range of cases pertinent to the helicopter flight envelope.

Nomenclature

a_2	=	coefficient of two-dimensional aerodynamic damping
C_M	=	pitching-moment coefficient
C_N	=	normal-force coefficient
C_P	=	pressure coefficient
C_W	=	work coefficient
c	=	airfoil chord, m
k	=	reduced frequency $c\omega/2U$
M	=	Mach number
Re	=	Reynolds' number based on airfoil chord length
T	=	nondimensional time period of oscillation
T_F	=	nondimensional duration of flap pulse signal
t	=	time, s
t_S	=	nondimensional start time of flap pulse signal
U	=	freestream velocity, m/s
x_c, y_c	=	non-dimensional airfoil pivot axis coordinates
α	=	angle of attack, deg
α_A	=	amplitude of airfoil oscillation, deg
α_M	=	mean angle of attack, deg
δ	=	flap deflection angle, deg
ψ	=	azimuth angle, deg
ω	=	oscillatory frequency, rad/s

Introduction

At high advance ratio and thrust coefficient a significant part of a helicopter's flight envelope is defined by the appearance of excessive pitch link loads as a consequence of stall flutter on the retreating blades.[1] Another part of the envelope is defined by shock waves forming on the advancing blades. The first harmonic of the blade angle of attack at around 75% span is close to sinusoidal, with high dynamic pressure and low angle of attack on the advancing side and low dynamic pressure and high angle of attack on the retreating one. The stall flutter boundary occurs when the retreating blades encounter dynamic stall.[2] Although stall flutter is not a physical boundary to the helicopter operation as such, the excessive pitch link loads resulting from stall flutter cause fatigue and vibration problems.

Dynamic stall on the retreating blades is associated with very high blade pitching moments and a loss of dynamic lift. The pitching moments prove to be the greatest problem as they cause excessive loads to be placed on the pitch links. The associated loss of dynamic lift is less important because, at high advance ratio, most of the helicopter rotor lift is generated between 65 and 85% span toward the front and rear of the rotor disc.

Although the fundamental physical phenomena causing dynamic stall are still not fully understood, successful blade designs that delay dynamic stall on helicopter blades have been developed. To gain a further performance improvement, it is timely and appropriate to consider flow control as a means of enhancing blade performance. Alleviation of the high transient pitching moments occurring during dynamic stall promises to extend the flight envelope of the helicopter rotor blade and its fatigue life.

The primary objective for most flow-control schemes for dynamic stall is to delay the stall onset. Active flow-control schemes show the most promise, as the flow-control device can be designed to affect the flow only on the retreating side, without compromising the performance of the blade on the advancing side. Several techniques have been employed to effect active control of dynamic stall, and these methods are briefly introduced here. Higher harmonic control (HHC) has been used to improve rotor performance.[3] In HHC the blade cyclic pitch mechanism is augmented with higher harmonics so that the lift generated by the rotor is more uniform over the rotor disc. By this mechanism the rotor's entry into stall is delayed because more rotor thrust can be generated for a given maximum blade angle of incidence than with a traditional once per-revolution cyclic pitch mechanism. HHC has, however, only achieved limited success in improving rotor stall performance[3] and is more commonly applied to control of blade vortex interaction.

Another strategy used to delay dynamic stall is to increase the maximum lift coefficient attainable by the airfoil section. Increasing the maximum lift coefficient can be achieved by adding camber; however, this is detrimental to advancing blade performance. However, an increase in section C_L can also be obtained with an oscillatory jet flap, without compromising the advancing blade performance. Lorber et al.[4] describe the use of an oscillatory jet flap incorporating a coanda surface at the rotor airfoil trailing edge. At

Presented as Paper 2003-0050 at the AIAA 41st Aerospace Sciences Meeting, Reno, NV, 6–9 January 2003; received 20 February 2003; revision received 24 July 2003; accepted for publication 20 August 2003.

*Research Assistant, Department of Aerospace Engineering. Member AIAA.
†Lecturer, Department of Aerospace Engineering.
‡Senior Lecturer, Department of Aerospace Engineering.

jet oscillations of roughly four per revolution[4] the unsteady pitching moment could be varied almost linearly with jet momentum coefficient, showing that this type of actuator could feasibly be used for control of blade pitching moments. A disadvantage of this, and any other jet-based flow-control actuator, is the pumping system required for each rotor blade.

Similarly, an increase in maximum section C_L can be obtained by delaying the separation process. Vortex generators are useful for delaying fixed wing separation, but these fixed vortex generators are not appropriate for a rotor application where the flow conditions vary around the rotor azimuth. Synthetic (or zero-mass) jets are small micro-electro-mechanical devices that produce a jet-like flow[5] and can be arranged in pairs to act like microvortex generators

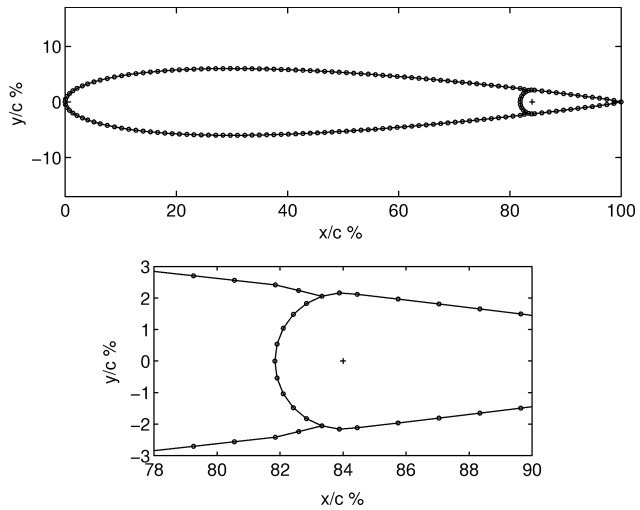

Fig. 1 Panel distribution on the NACA 0012 airfoil and the detail of the notches appearing caused by the introduction of the flap.

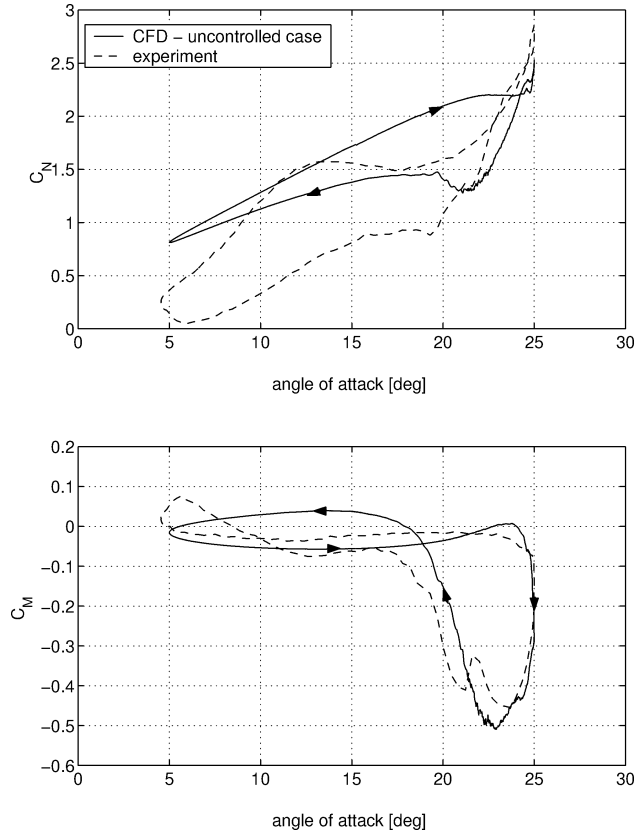

Fig. 2 Comparison of the experimental and numerical C_N-α, C_M-α curves.

or can also be used to modify the effective aerodynamic shape of the airfoil by creating a small recirculation region close to the airfoil surface.[6] These synthetic jets are to be preferred for a rotor application because they obviate this need for a pumping system along each blade, although their electrical power requirements can be significant.

Active flow-control techniques using actively deforming airfoil designs have also been studied,[7–9] and these works often consider a leading-edge actuator. A technique that is very promising for delaying the onset of dynamic stall is dynamically deforming leading-edge control (DDLE) as discussed by Chandrasekara et al.[10] Here, the airfoil leading-edge geometry is actively deformed prior to entering dynamic stall. As the dynamic-stall instability is essentially a leading-edge phenomenon for most rotor sections, this technique is able to delay the onset of the stall by several degrees of incidence, for a given airfoil pitch rate. For example, Chandrasekara et al.[10] reported an increase of 4 deg in dynamic-stall incidence for a given pitch rate of a NACA 0012 profile. Yu et al.[11] in a numerical study have also shown that the lift and moment hysteresis occuring during

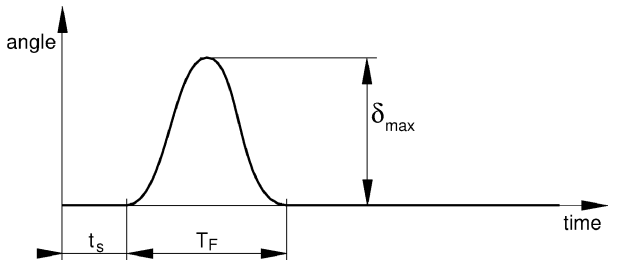

Fig. 3 Parameters of the pulse signal.

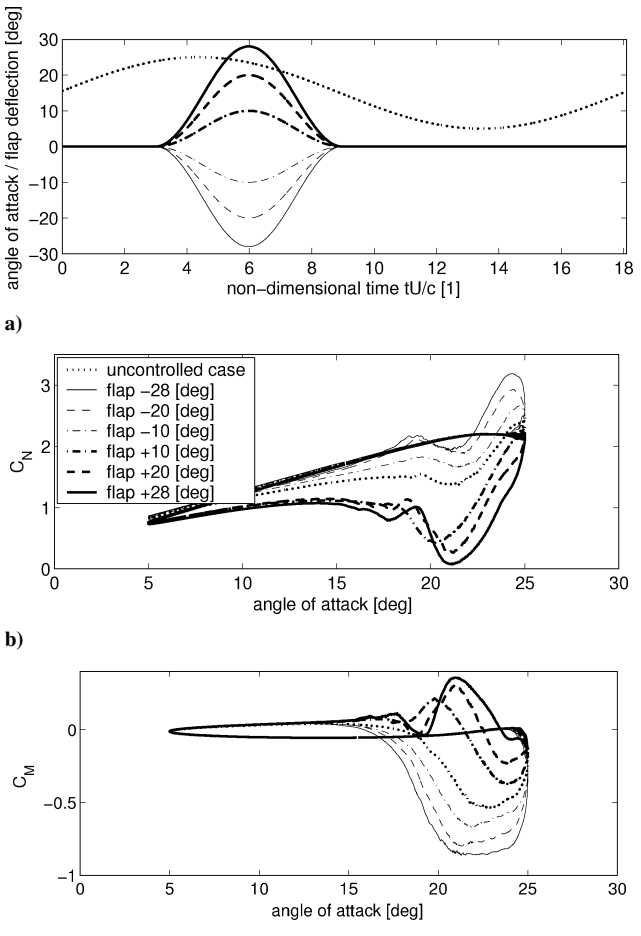

Fig. 4 Effect of the flap deflection amplitude δ_{max} on the C_N-α and C_M-α curves.

dynamic stall can be reduced with a DDLE airfoil. Although the leading edge is the most aerodynamically appropriate location for a flow-control actuator, and although smart materials might conceivably aid in the manufacture of a DDLE airfoil, there are practical difficulties in citing an actuator at the leading edge because of the severe environment there. Most rotor blades are equipped with a titanium, or steel, erosion shield at the leading edge, for example.

Although these devices have shown some promise in delaying the onset of dynamic stall, the objective of the current work is to use a trailing-edge-flap flow-control actuator to reduce the pitching-moment loads associated with stall, once stall has already initiated. Also, because of the severe environment at the leading edge a more practical site for building a flow-control actuator is at the trailing edge. Dynamic stall is essentially a leading-edge phenomenon, so that the most an actuator at the trailing edge could provide is a mitigation of the effects of the process rather than to delay dynamic stall itself. Indeed, pulse actuation of flaps has shown promise for the simpler, but related, application of suppression of stall flutter of a bridge section,[12] and dynamic scheduling of flaps has been successful in improving the performance of maneuvering aircraft.[9] An additional advantage of trailing-edge flaps has been demonstrated by Celi,[13] who showed that these can also serve as emergency control surfaces in the case of pitch link failure.

The pragmatic objective of the current work is to mitigate the excessive pitching-moment break and associated loss of pitch damping occurring during dynamic stall by forcing the flow with a pulsed trailing-edge flap. Pulsing a flap at the trailing edge is possible because the dynamic pressures are very low on the retreating side where dynamic stall is a problem.

The present work will investigate this flow control strategy by using a computational-fluid-dynamics (CFD) simulation of an airfoil undergoing sinusoidal pitch oscillation. This sinusoidal oscillation models the first harmonic of an actual rotor blade angle-of-attack history as it rotates around the azimuth in forward flight. Although the reduced pitch rate changes over an actual rotor disc, the present study will use a constant reduced pitch rate for computational convenience. The test case selected, however, will be representative of the dynamic-stall conditions experienced by a typical rotor blade at one extreme of the flight envelope (high thrust coefficient and advance ratio). It is the objective of the work to understand the mechanism of the flap/dynamic stall vortex interaction by analyzing the numerical results and, based on this, to suggest an optimum flap strategy, which will minimize blade pitching moments while maximizing dynamic lift.

Two-Dimensional Aerodynamic Damping

Stall flutter and excessive pitch link loads occur when the aerodynamic damping becomes negative. The coefficient of two-dimensional aerodynamic damping will be evaluated throughout this paper according to the definition of Carta[1] as

$$a_2 = -C_W \big/ \pi \alpha_A^2 \tag{1}$$

where C_W is the work coefficient expressed in terms of the integral of the moment coefficient, that is,

$$C_W = \oint C_M \, \mathrm{d}\alpha \tag{2}$$

This means that anticlockwise loops in a $C_M - \alpha$ curve contribute positive values to the cycle aerodynamic damping, whereas clockwise loops negative ones.

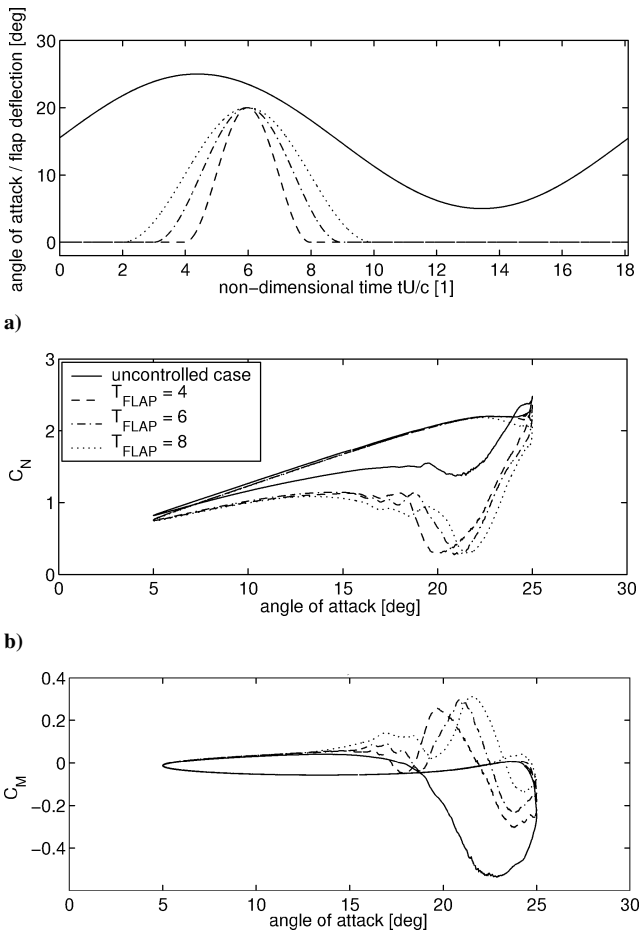

Fig. 5 Effect of the flap actuation duration time T_F on the C_N-α and C_M-α curves.

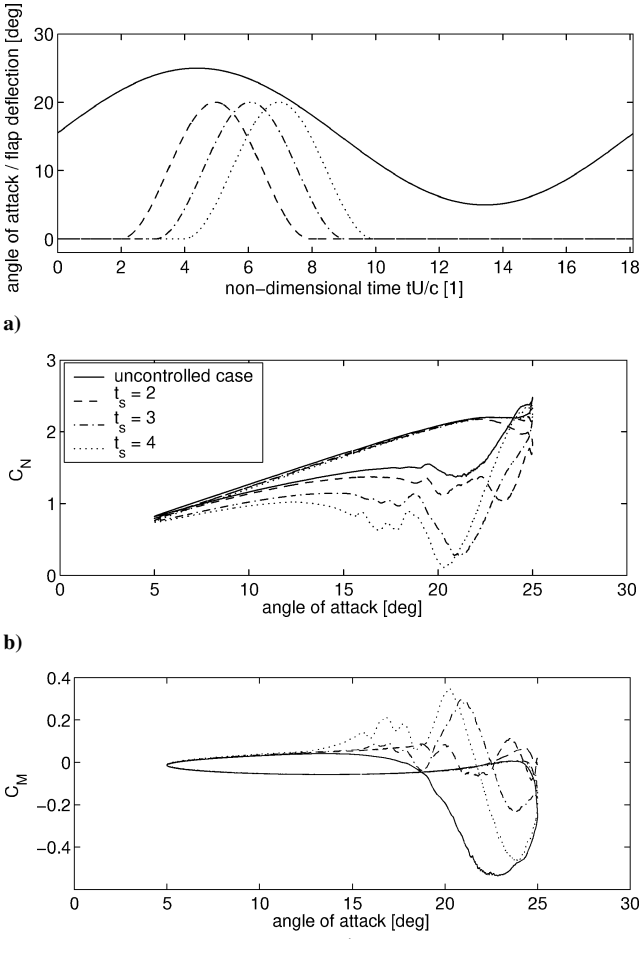

Fig. 6 Effect of the flap actuation start time t_s on the C_N-α and C_M-α curves.

Test Case

A test case exhibiting severe negative damping was selected as the reference case from the experimental work of Galbraith.[14] In the experiment the model geometry was a NACA 0012 airfoil oscillating in a sinusoidal motion of $\alpha(t) = 15 \text{ deg} + 10 \text{ deg} \sin(\omega t)$ at the reduced frequency $k = 0.173$, in the freestream flow conditions of $M = 0.117$ and $Re = 1{,}463{,}296$. (The mechanism of dynamic stall has been shown to be largely independent of Reynolds number.[15–17]) In the computational approach the airfoil chord was set to unity, and a 16% chord flap was also introduced at the trailing edge. A trailing-edge flap of this size was considered to be realistic, causing little disruption to the structural integrity of the blade. The modeling of the flap necessitated the introduction of two "notches" on each side of the airfoil (Fig. 1). These were introduced purely for computational convenience and were a requirement for the incompressible numerical method to maintain constant volume of the flapped airfoil during the simulations.

Numerical Method

The DIVEX discrete vortex method[18] was used for the simulations. The advantage of using such method lies in its suitability to capture vortex-dominated flows accurately and that neither a transform mapping nor prespecification of the separation point is required. The method is grid free, which is advantegous for moving multibody applications, such as the present flapped airfoil in oscillatory motion. In the DIVEX code the two-dimensional incompressible Navier–Stokes equations are solved in a vorticity/stream function form. A thin layer near the airfoil, the control zone, is the source for the vortices, which arise there from the no-slip condition on the solid boundary. A Lagrangian scheme is used to describe the convection of the vortices released from the control zone, and a random-walk method[19] is employed to simulate diffusion. Thus, second-order temporal and spatial accuracy was achieved. The surface of the body is discretized into main panels and subpanels, the latter used to represent the leading edge accurately and to define the vorticity within the control zone. The boundary condition is satisfied by enforcing zero mass flow through the main panels. In the present work the airfoil surface (including the flap and the notches) was represented by 167 panels, with five subpanels defined between successive main node points. The vortex core radius, vortex creation distance above the surface and size of control zone were empirically specified and were of the same order of magnitude as the panel lengths.

Validation of the Numerical Method

The time-averaged numerical results, considering 10 cycles, were validated in terms of angular variation of the pitching-moment C_M and normal-force C_N coefficients for the clean, uncontrolled, airfoil (Fig. 2). Good comparison was obtained for the phasing of the events, that is, the timing of the lift stall and pitching-moment stall. The magnitude of these parameters, especially that of C_M, was also well predicted and, although the poststall value of C_N appeared to

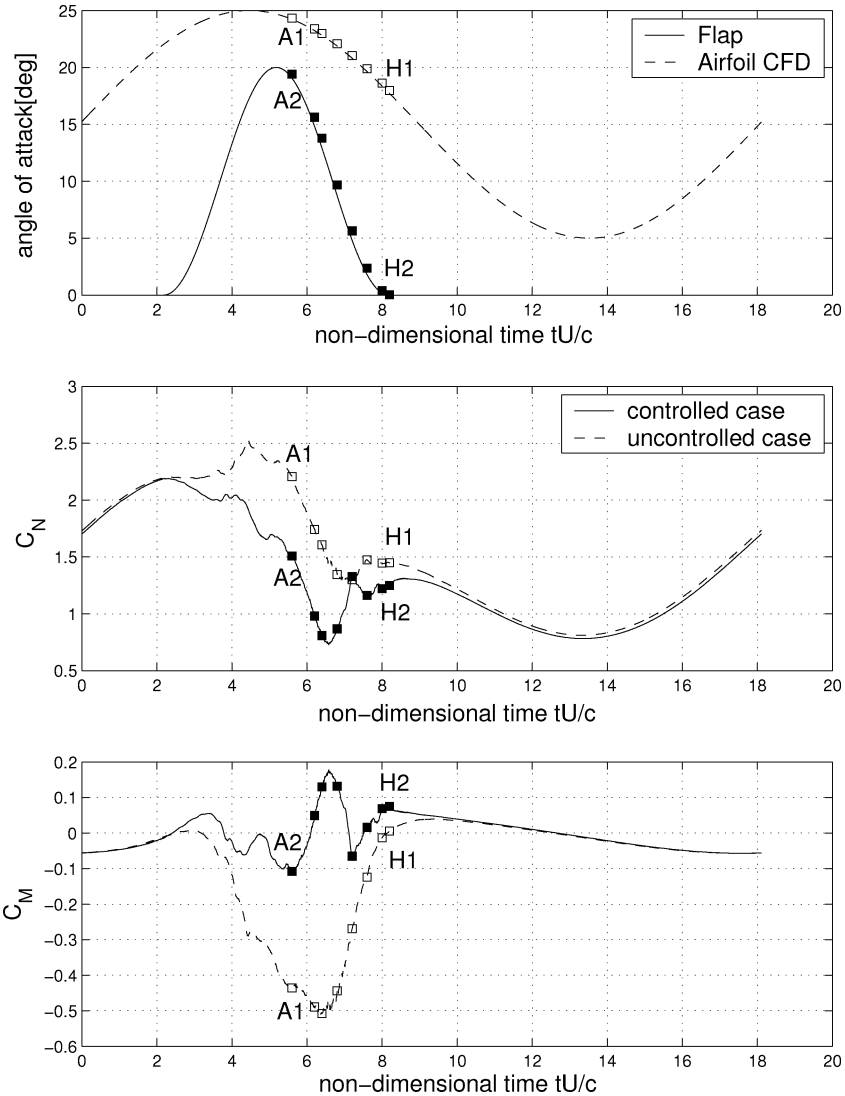

Fig. 7 Time-averaged C_N and C_M histories showing the reduction of negative damping by employing the flap actuation of $\delta_{max} = 20$ deg, $T_F = 6$, and $t_s = 2.200$.

be overpredicted, the computational results shared the same trend with the experiment. The second loop of the $C_M - \alpha$ curve has a clockwise sense and therefore will represent negative aerodynamic damping, reduction of which is the primary aim of using the flap flow control.

Flap Actuation

The actuation employed was a brief pulse of the 16% chord trailing-edge flap. The choice of such flap scheduling was motivated by the idea of counteracting the undesired pitching-moment stall for only a certain, and relatively small, azimuthal range of the rotor blade travel while maintaining the benefits of the original rotor-blade behavior outside this range. The flap was actuated at a time representative of the retreating side of the rotor, which experiences low dynamic pressure. The pulse signal was represented by the function of $\delta(t) = \delta_{\max}[1 - \cos(t/T_F)]$ (Fig. 3) and was tested in terms of three parameters: the pulse amplitude $\delta_{\max}$, the pulse start time t_s, and the duration of the actuation T_F. The effects of these parameters, in relation to a chosen base case of $\delta_{\max} = 20$ deg, $t_s = 3$, and $T_F = 6$, were evaluated individually.

Effect of Flap Deflection $\delta_{\max}$

Both upward and downward flap deflections were considered, with the results (Fig. 4) leading to the following observations:

1) Only upward (positive) flap deflections can lead to the reduction of negative damping, that is, the second loop of the $C_M - \alpha$ curve.

2) The larger the flap deflection the more efficient the reduction mechanism is.

3) The larger the flap deflection, the larger C_M overshoot appears on the downstroke of the airfoil motion.

4) For positive flap deflections the magnitude of the deflection has no effect on the maximum value of dynamic lift.

5) The lift in the dynamic-stall regime is significantly smaller for the upward flap deflections than in the uncontrolled case.

Effect of Flap Duration T_F

Three flap actuation durations were considered, with coinciding peaks (Fig. 5). It was found that 1) longer durations reduce negative damping more effectively; however 2) they also generate larger C_M overshoots on the downstroke of the airfoil motion, and 3) the flap duration has no effect on the maximum value of dynamic lift.

Effect of Flap Start Time t_s

Figure 6 shows the results for three different flap start times. As can be seen, 1) although earlier actuations reduce negative damping more effectively, they also lead to significant loss in the maximum achievable dynamic lift, and 2) the later the actuation the greater the poststall lift loss is.

Optimum Flap Actuation

Based on the preceding tests, one could conclude that the optimum flap actuation should incorporate positive flap deflections of medium amplitude ($\delta_{\max} = 20$ deg) so that large overshoots of C_M are avoided; medium to long durations ($T_F = 6$–8) so that negative damping is reduced effectively; and relatively early timing (between $t_s = 1$ and 3) so that a good compromise between reducing negative damping and maximizing dynamic lift is achieved and that the actuation takes place in the third and fourth azimuthal quarters of the rotor, where the dynamic pressure is the lowest.

A suitable compromise satisfying all of these conditions was found by employing a $\delta_{\max} = 20$ deg, $T_F = 6$, and $t_s = 2.200$ actuation as shown in Figs. 7 and 8. This particular flow-control strategy altered the value of two-dimensional aerodynamic damping from a severe negative value, $a_2 = -0.1682$, to a favorable positive one, $a_2 = 0.2546$, while maintaining as much as 89% of the original dynamic lift. Hence, this case was used for the analysis of the trailing-edge-flap flow-control mechanism.

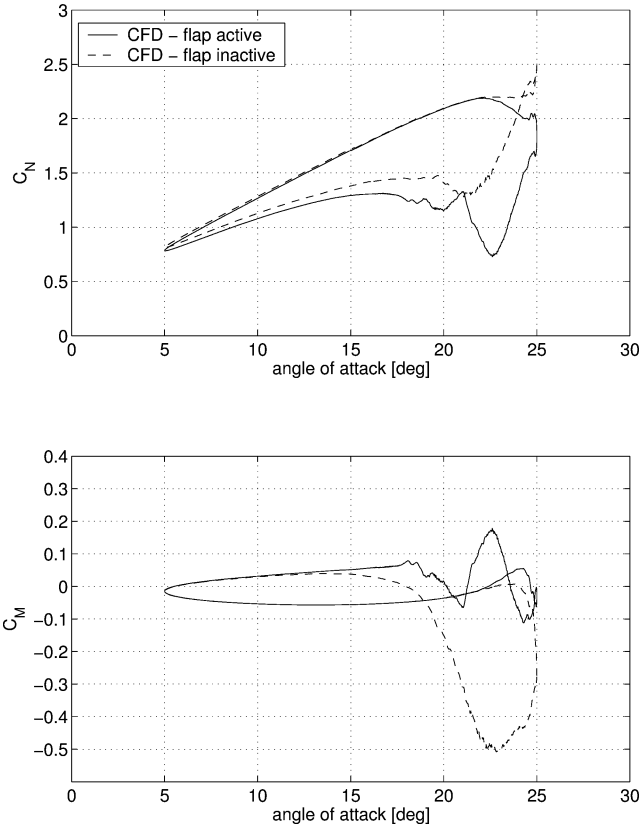

Fig. 8 C_N-α and C_M-α loops showing the reduction of negative damping by employing the flap actuation of $\delta_{\max} = 20$ deg, $T_F = 6$, and $t_s = 2.200$.

Flow Analysis

To enable the application of the preceding flow-control strategy to other, more general, points in the helicopter flight envelope, the flow-control mechanism had to be analyzed and understood first so that the general criteria driving the flap actuation could be formulated. A sequence of flow-visualization frames, taken at the same time instants in the uncontrolled and controlled cases, is shown in Fig. 9. The comparison of the surface pressure distributions is also provided for each frame in the third column. The vector plots show only that part of the cycle which details the features interesting from the present flow-control point of view, that is, the dynamic-stall behavior in the vicinity of the trailing edge flap. The time positioning of the frames is indicated in Fig. 7. (The endpoints A and H are labeled on Fig. 7, with the squares in between referring to points B, C, D, E, F, and G.)

Uncontrolled Flow

Figure 9a1 depicts a large dynamic-stall vortex (DSV) convecting downstream over the airfoil. This vortex has a clockwise direction and generates extra suction over the upper surface of the blade section, as indicated by the C_P plot in Fig. 9a3. (The kink in the C_P plots toward the trailing edge appers there because of the notches.) As the DSV approaches the trailing edge of the airfoil, a trailing-edge vortex (TEV) is generated there. This appears as a result of the mass influx from the high-pressure airfoil lower surface to the upper surface, which at this stage is dominated by the DSV suction in the vicinity of the trailing edge. The TEV rolls up in an anticlockwise direction and forms a pair of counter-rotating vortices with the DSV. Another role of the TEV is that it feeds the dynamic-stall vortex with flow originating from the freestream. All of these features regarding the formation of the TEV have also been observed experimentally.[20–23]

As the DSV continues its migration downstream (Figs. 9b1 and 9c1), the TEV also grows in strength and size, causing another suction peak to appear over the trailing edge of the airfoil (Figs. 9b3

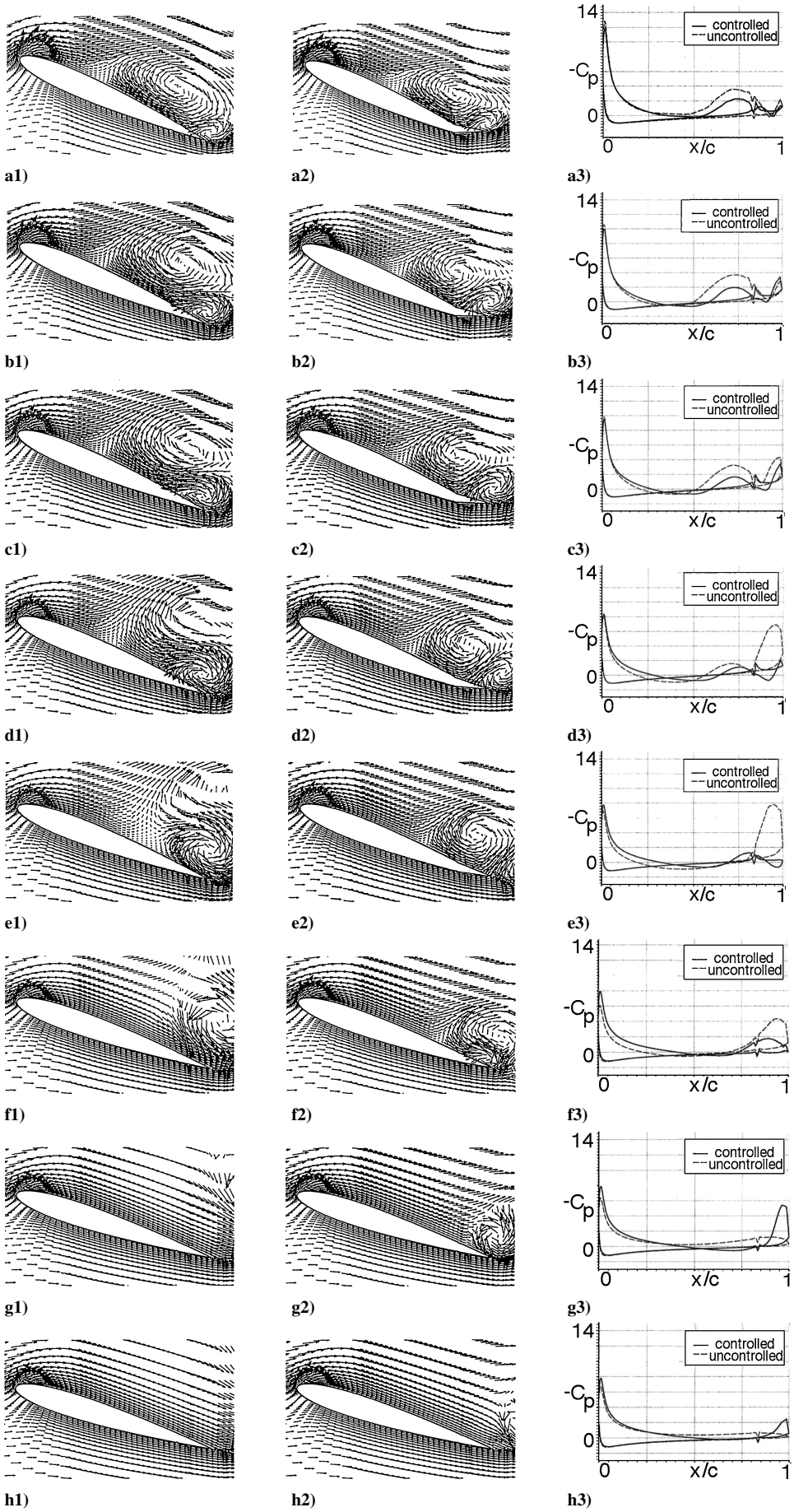

Fig. 9 Vector plots for the uncontrolled (first column) and controlled (second column) cases of dynamic stall, corresponding to points A1–H1 and A2–H2 from Fig. 7, respectively. Third column shows the comparison of the C_P distributions over the airfoil surface.

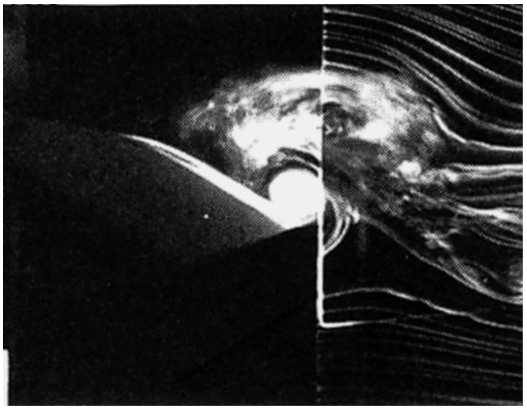

a)

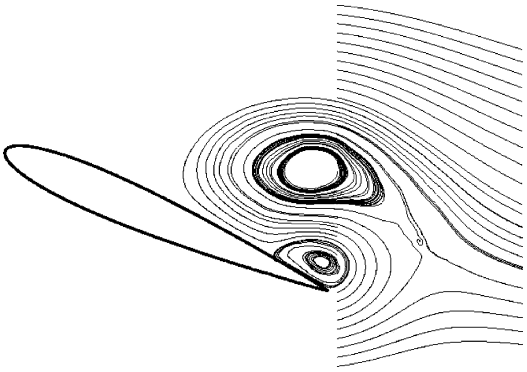

b)

Fig. 10 Comparison of a) the flow-visualization photograph of Panda and Zaman[23] [$k = 0.2$, $\alpha(t) = 15$ deg + 10 deg sin(ωt)] and b) the instantaneous streamlines of frame D1 from Fig. 9d1. The smoke wire and the source line of the streamlines were both placed downstream of the trailing edge.

and 9c3). Acting on a long arm to the pivot axis, this will have a quite significant contribution to the negative pitching moment, which reaches its minimum in frames B1 and C1 (Fig. 7).

As the DSV attempts to complete its downstream convection along the shortest possible path, it is seen to "roll over" around the TEV, that is, detaching from the airfoil surface (Figs. 9d1, and 9e1). The mutual position of the two vortices can be confirmed from flow-visualization frames available from the experimental work of Panda and Zaman,[23] in which a nearly identical configuration to the current one was tested. A comparison of the experimental photograph and the corresponding CFD frame is avilable in Fig. 10, from which it is apparent that the distortion of the DSV to a characteristic elliptical shape was correctly captured by the numerical method.

This is an important observation because it means that the large negative pitching moments experienced at this stage of the flow (points B1–E1 in Fig. 7) are caused not just by the DSV, which is already detached from the airfoil surface, but also by the TEV. Hence, if one aims to reduce the large nose-down pitching moments and the associated negative aerodynamic damping on an oscillating airfoil, it makes sense to attempt to influence the behavior of the TEV rather than that of the DSV.

The wash down of the vortex pair is completed by Figs. 9f1–9h1, leading to a quick recovery of the pitching moment to positive values again (Figs. 9f3–9h3 and points F3–H3 in Fig. 7).

Controlled Flow

Figures 9a2–9h2 show the sequence of vector plots for the controlled case. Note that the time instants for these frames are identical to those for the uncontrolled one, as indicated in Fig. 7 (points A2–H2).

In Fig. 9a2 the DSV can be seen again convecting downstream along the airfoil upper surface, and as it approaches the trailing-edge region it induces a trailing-edge vortex there. However, the TEV will this time be somewhat weaker than in the uncontrolled case because of the upward deflected flap. This will lead to lower pressure on the airfoil lower surface and hence yield smaller pressure difference between the upper and lower surfaces in the trailing-edge region (Fig. 9a3). Therefore, the partial feeding of the DSV will be less effective too, yielding less suction and smaller nose-down pitching moments because of the DSV than before (point A2 in Fig. 7).

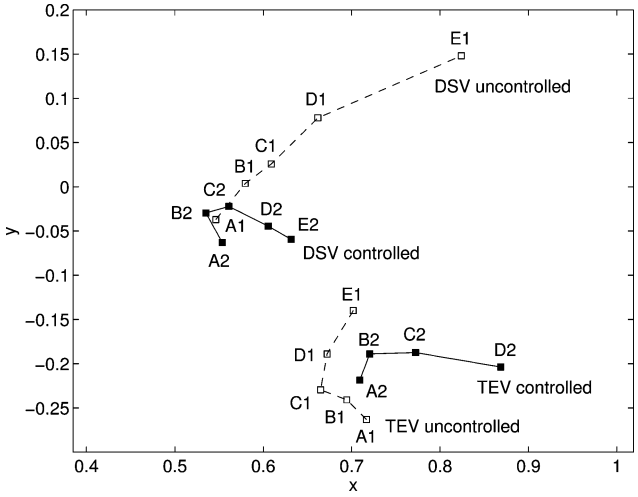

Fig. 11 Evolution of the DSV and TEV vortex core locations (coordinate system origin located at the airfoil pivot axis x_c, y_c).

The most important effect of the flap flow control is, however, that it displaces the TEV to a much higher position than in the uncontrolled case. This is apparent from Fig. 11, showing the vertical locations of the DSV and TEV vortex cores for the uncontrolled and controlled cases.

It is clear that the vertical distance between these two vortices is much smaller when the flap is deflected upward, forcing the DSV to push the TEV downstream off the trailing edge (Figs. 9b2–9e2). The suction effect associated with the TEV will therefore diminish in this case (solid lines in the C_P plots in Figs. 9b3–9e3), along with the associated large nose-down pitching moments and negative damping (points B2–E2 in Fig. 7).

As the DSV passes the trailing edge, another trailing-edge vortex is generated for a short period of time but with insignificant effect (Fig. 9f2) until the flow finally settles as the DSV is washed down in Figs. 9g2–9h2.

The overshoot in the C_M history (points C2–D2 in Fig. 7) coincides with the time instant when the TEV passes the trailing edge. At that point the suction caused by the TEV suddenly disappears, and the flow in the mixing layer of the vortex pair acts perpendicularly on the trailing edge (see Figs. 9d2 and 9e2 and the C_P rise on the upper surface of the flap in Figs. 9d3 and 9e3). Finally, the lift in the controlled case stalls earlier and is constantly lower for the duration of the flap actuation because of the upward deflections involved.

Extension of Applicability

Although the suggested flow-control strategy appeared to work well for one particular airfoil configuration, it is imperative to show that the method can be successfully applied for a range of other conditions typical of a helicopter flight envelope. For a range of reduced frequencies and mean incidence angles, a three-dimensional surface of aerodynamic damping can be constructed, such as the one available from Carta.[1] To demonstrate the feasibility of the present flow-control technique for a range of configurations, two orthogonal lines from such a surface were explored, one for varying k and one for varying α_M.

For the flap actuations along these lines, a self-similar flap strategy was applied, that is, the T_F/T ratio was kept $\frac{1}{3}$ as in the base case. The start time t_S was adjusted to achieve the maximum possible reduction in aerodynamic damping, and $\delta_{\max}$ was set in a manner

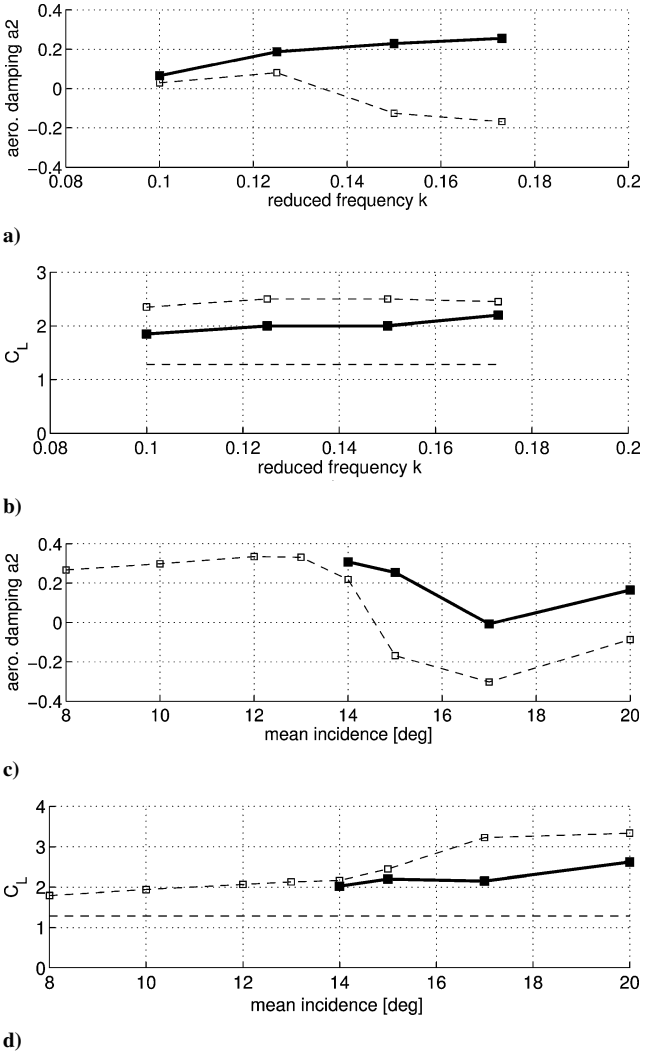

Fig. 12 Evolution of aerodynamic damping and maximum lift coefficient for controlled and uncontrolled flows at varying reduced frequencies and varying mean incidence: ——, controlled flow; - -□- -□, uncontrolled flow, and – – –, static C_L.

so that the maximum flap-deflection angle relative to the freestream would be constant in each case, $\alpha_{\max} - \delta_{\max} = 5$ deg.

The results for the variations of a_2 by k and α_M are shown in Figs. 12a and 12c, respectively. In both cases the large negative values of aerodynamic damping could be altered to positive ones while maintaining at least 80% of the original, uncontrolled dynamic lift in the majority of the cases (shown in Figs. 12b and 12d.

A practical aspect of the proposed flow-control technique regards the timing of the flap. Because the actuation always occurs between the mean and the maximum incidence angles, it will actually fall into the third quarter of the azimuthal range (180–270 deg), in which the dynamic pressure on the blade is relatively low. (The minimum dynamic pressure occurs around $\psi = 270$ deg). Equally, the retraction of the flap would occur in the fourth quarter (270–360 deg), so that the actuation of the flap would require relatively low energy.

It is expected that future work on this project will employ a pressure transducer towards the leading edge of the airfoil as a means of inferring the blade angle of attack and hence the appropriate flap actuation timing.

Conclusions

The preceding results are promising and show that a pulsed trailing-edge flap has the potential of improving the rotor performance by removing the large pitching moments associated with blade dynamic stall at the extremes of the helicopter flight envelope.

Systematic study of the flap actuation parameters showed that only upward flap deflections could lead to the reduction of aerodynamic damping. The optimum duration of the flap pulse was found around $\frac{1}{3}$ of the time period of oscillation, with the start time typically between the mean and the maximum airfoil incidence angles, i.e in the 3rd quarter of the azimuth.

Detailed analysis of the flowfield showed that the dynamic-stall vortex (DSV) and the trailing-edge vortex (TEV) form a pair of counter-rotating vortices during dynamic stall. In the uncontrolled case the DSV rolls over the TEV as it convects downstream, whereas in the controlled case it pushes the TEV downstream off the trailing edge. This is because of the higher location of the TEV when the flap is actuated. Because large negative aerodynamic damping was found to be associated with the presence of TEV, this could be successfully reduced by applying the suggested trailing-edge-flap flow control.

Shown too was that the suggested flow-control strategy could be successfully employed to other configurations in the simulated helicopter flight envelope. For these cases self-similar flap pulse signals can be used, and only the timing of the flap has to be adjusted. The start and the end times of the actuations fell always into the third and fourth quarter of the azimuth, respectively, where in an actual helicopter rotor the dynamic pressure is close to its minimum, and so realistic flap actuators would be expected to require relatively low energy.

Acknowledgments

The authors acknowledege the support of the United Kingdom Engineering and Physical Sciences Research Council on Grant GR 39290/01 and the advice and assistance of Richard B. Green of the University of Glasgow and Ian W. Kaynes of QinetiQ, Farnborough, England, United Kingdom.

References

[1]Carta, F., "An Analysis of the Stall Flutter Instability of Helicopter Rotor Blades," *Journal of the American Helicopter Society*, Vol. 12, No. 4, 1967, pp. 1–18.

[2]McCroskey, W., "Unsteady Airfoils," *Annual Review of Fluid Mechanics*, Vol 14, 1982, pp. 285–311.

[3]Nguyen, K., "Active Control of Helicopter Blade Stall," *Journal of Aircraft*, Vol. 35, No. 1, 1998, pp. 91–98.

[4]Lorber, P., Carta, F., and Carlson, R., "The Aerodynamics of an Oscillating Jet Flap," *Journal of the American Helicopter Society*, Vol. 34, No. 2, 1989, pp. 24–32.

[5]Greenbaltt, D., and Wygnanski, I., "Dynamic Stall Control by Periodic Excitation, Part 1: NACA 0015 Parametric Study," *Journal of Aircaft*, Vol. 38, No. 3, 2001, pp. 430–438.

[6]Greenbaltt, D., Nishri, B., Darabi, A., and Wygnanski, I., "Dynamic Stall Control by Periodic Excitation, Part 2: Mechanisms," *Journal of Aircaft*, Vol. 38, No. 3, 2001, pp. 439–447.

[7]Chandrasekhara, M., Wilder, M., and Carr, L., "Compressible Dynamic Stall Control: Comparison of Two Approaches," *Journal of Aircraft*, Vol. 38, No. 3, 2001, pp. 448–453.

[8]Laurie, L., and Farokhi, S., "Separated Flowfield and Lift on an Airfoil with an Oscillating Leading-Edge Flap," *Proceedings of the 11th Applied Aerodynamics Conference*, AIAA, Washington, DC, 1993, pp. 190–199.

[9]Rennie, R., and Jumper, E., "Dynamic Leading-Edge Flap Scheduling," *Journal of Aircraft*, Vol. 34, No. 5, 1997, pp. 606–611.

[10]Chandrasekara, M., Wilder, M., and Carr, L., "Unsteady Stall Control Using Dynamically Deforming Airfoils," *AIAA Journal*, Vol. 36, No. 10, 1998, pp. 1792–1800.

[11]Yu, Y., Lee, S., McAlister, K., and Tung, C., "Dynamic Stall Control for Advanced Rotorcraft Application," *AIAA Journal*, Vol. 33, No. 2, 1995, p. 289.

[12]Lecce, L., Selvaggi, E., Nicolosi, F., Baruffo, M., and Abate, A., "New Experimental Stall Flutter Active Control of a Bridge Section," *CEAS/AIAA/ICASE/NASA Langley International Forum on Aeroelasticity and Structural Dynamics*, edited by W. Whitlow and E. N. Todd, NASA CP 209136, 1999, pp. 311–324.

[13]Celi, R., "Stabilization of Helicopter Blades with Severed Pitch Links Using Trailing-Edge Flaps," *Journal of Guidance, Control, and Dynamics*, Vol. 26, No. 4, 2003, pp. 585–592.

[14]Galbraith, R., Gracey, M., and Gilmour, R., "Collected Data for Tests on a NACA 0012 Aerofoil. Volume II: Pressure Data from Oscillatory Tests," Glasgow Univ., Aero Rept. 9208, Glasgow, Scotland, U.K., Feb. 1992.

[15]VanDommelen, L., and Shen, S., "The Spontaneous Generation of the Singularity in a Separating Laminar Boundary Layer," *Journal of Computational Physics*, Vol. 38, 1982, pp. 124–140.
[16]Acharya, M., and Metwally, M., "Unsteady Pressure Field and Vorticity Production over a Pitching Airfoil," *AIAA Journal*, Vol. 30, 1992, pp. 403–411.
[17]Doligalski, T., Smith, C., and Walker, J., "Vortex Interactions with Walls," *Annual Review of Fluid Mechanics*, Vol. 26, 1967, pp. 573–616.
[18]Lin, H., and Vezza, M., "Discrete Vortex Method for Simulating Unsteady Flow Around Pitching Airfoil, *AIAA Journal*, Vol. 35, No. 3, 1997, pp. 494–499.
[19]Chorin, A., "Numerical Study of Slightly Viscous Flow," *Journal of Fluid Mechanics*, Vol. 57, No. 4, 1973, pp. 785–796.
[20]Robinson, M. C., Helin, H. E., and Luttges, M. W., "Control of Wake Structure Behind an Oscillating Airfoil," AIAA Paper 86-2282, Aug. 1986.
[21]Ohmi, K., Coutanceau, M., Daube, O., and Loc, T. P., "Further Experiments on Vortex Formation Around Oscillating and Translating Airfoil at Large Incidences," *Journal of Fluid Mechanics*, Vol. 225, 1991, pp. 607–630.
[22]Shih, C., and Lourenco, L., Van Dommelen, L., and Krothapalli, A., "Unsteady Flow past an Airfoil Pitching at a Constant Rate," *AIAA Journal*, Vol. 30, No. 5, 1992, pp. 1153–1161.
[23]Panda, J., and Zaman, K., "Experimental Investigation of the Flow Field of an Oscillating Airfoil and Estimation of Lift from Wake Surveys," *Journal of Fluid Mechanics*, Vol. 265, 1994, pp. 65–95.

W. Devenport
Associate Editor